Australian Earthquake Engineering Society
2023 National Conference, 23-25 November 2023
Brisbane, Queensland, Australia

Updates to the Somerville et al. (2009) Ground Motion Model for Australia Using Broadband Ground-Motion Simulations

Jeff Bayless[1], Paul Somerville[2], Hong Kie Thio[3], María Elisa Ramos-Sepúlveda[4]

1. *AECOM, Los Angeles, jeff.bayless@aecom.com*

2. *AECOM, Los Angeles, paul.somerville@aecom.com*

3. *AECOM, Los Angeles, hong.kie.thio@aecom.com*

4. *University of California, Los Angeles, mariaramos1@g.ucla.edu*

Abstract

Changes to seismic hazard models with time reflect our increasing knowledge of earthquake source and ground motion characteristics in Australia. Because considerable strong ground motion recordings have been collected and analysed in Australia in recent years, it is important to update the ground motion models (GMMs) which underpin the seismic hazard results and, ultimately, drive the design ground motions in future engineering standards and guidelines. The Somerville et al. (2009; Sea09) GMMs for Australia are due for improvement by taking advantage of these ground motions recorded in the past decade-plus. This paper describes ongoing changes to the Sea09 ground motion model, and as a result how seismic hazard results for engineering projects may be impacted.

Updates to Sea09 utilise broadband strong motion simulations to account for earthquake source and crustal structure properties of Australia. The simulations are validated with data recorded in Cratonic and non-Cratonic Australia (provided by Geoscience Australia; Ghasemi and Allen, 2021) and utilise contemporary methods (Graves and Pitarka, 2015). The validations compare attenuation, goodness of fit, and spectral shapes of ground motions recorded in twelve Cratonic region earthquakes. Large suites of forward simulations are used to extrapolate the model to larger earthquake magnitudes that typically control design ground motions but for which no Australian data are available.

Comparisons with recently recorded ground motions in Australia have revealed that refinements to the distance and depth scaling components of Sea09 provide a better fit to those data. The Cratonic and non-Cratonic region data show minimal differences in path and magnitude scaling, and similar spectral shapes. One exception is the amplification of response spectral periods between 1 and 3 seconds due to R_g waves from shallow source depths in Cratonic regions. The vertical component ground motion data is used to derive a vertical-to-horizontal (V/H) spectral ratio model for Cratonic Australia. When finalised, the unified model (Cratonic and non-Cratonic) will contain all of these features.

Keywords: Ground motion models, ground motions simulations, seismic hazard

1 Introduction

One critical component of a seismic hazard assessment (SHA) is the selection of ground motions models (GMMs), because the SHA results are highly dependent on these models. The Somerville et al. (2009; Sea09) GMMs for Australia were based on ground motion simulations, and then checked for consistency with the recorded ground motions of the moment magnitude (**M**) 4.47 Thompson Reservoir earthquake of 1996. In the course of the National Seismic Hazard Assessment (NSHA18; Allen et al., 2018), Geoscience Australia assessed the performance of existing ground motion models in predicting recorded ground motions in Australia (Ghasemi and Allen, 2018). They demonstrated that Sea09 could be improved by taking advantage of ground motions recorded in the past decade-plus. The expectation of change in ground motion models is embodied in Section 2.5 of the 2019 ANCOLD seismic guidelines, which states that it is unlikely that a SHA more than about 10 years old is reliable. Changes to seismic hazard models with time reflect our increasing knowledge of earthquake source and ground motion characteristics in Australia.

This paper describes how the Sea09 ground motion model has changed, and as a result how SHA results for engineering projects may be impacted. Comparisons with recently recorded ground motions in Australia have revealed that refinements to the distance and depth scaling components of the model provide a better fit to those data. This update also involves ongoing earthquake ground motion simulations; these are validated using the recorded ground motion data and are used to extrapolate the model to larger earthquake magnitudes that typically control design ground motions but for which no Australian data are available.

2 Earthquake Data

We compiled a Cratonic earthquake ground motion database including waveform data from Geoscience Australia (Ghasemi and Allen, 2021), who provided instrument corrected recordings for events occurring within Cratonic regions, and from IRIS (https://ds.iris.edu/wilber3/). We removed events with **M** less than 3.0, recordings with distance greater than 600 km, and those identified as clipped, with poor signal to noise ratio, or other artifacts. Recordings without both orthogonal horizontal components were also removed. The resulting database contains 536, homogeneously processed, ground motion records from 83 events recorded by 143 unique stations. Since compiling this database, additional data have been recorded, such as events from the 2022-23 Arthur River swarm (Miller et al., 2023), and these will be included in future database updates to the extent possible.

The Cratonic ground motion database includes three earthquakes with more than 80 records, these are the **M**3.91 event on 2019 May 30, the **M**4.71 event on 2019 May 30, and the **M**4.96 event on 2019 August 1. These three earthquakes were located within the Northern Australian Craton and were recorded by the temporary AusARRAY deployment (Gorbatov et al., 2020). The remaining 80 earthquakes in the database used in this study have fewer than 14 recordings within 600 km. There are 34 total events with **M** ≥ 4.0 and 33 events with 3.5 ≤ **M** < 4.0. The 5% damped, horizontal component pseudo-spectral accelerations (RotD50; Boore, 2010) are calculated from two-component band-passed acceleration time histories using the pyRotd python library (Kottke, 2018).

The cut-and-paste (CAP) method for retrieving earthquake source parameters (Zhao and Helmberger, 1994; Tan et al., 2010) breaks three-component data into regional P waves (*Pnl,* consisting of refractions along the crust–mantle interface, Pn, and the crustal P arrivals and PmP along with various S segments at distances from 150 to 1400 km; Helmberger and Engen, 1980*)* and surface wave segments, and models them separately, so imperfect 1-dimensional Green's functions can be effectively used to determine source parameters. We utilize the CAP method on 9 of the 12 events listed in Table 1 to improve our estimates of **M**, focal depth, focal mechanism, and location, resulting in some differences between our source parameter estimates and those from the GA and global catalogues. Metadata for events with EQID 13,

49 and 55 (bold in Table 1) are from Ghasemi and Allen (2021). Figure 1 shows the results of this method, using a six-station inversion, for the August 1, 2019 Northern Territory event. This inversion has a minimum waveform misfit error at 2 km depth (centre left panel), and a northeast p-axis orientation consistent with Hillis & Reynolds (2000) (top left). The event and recording station locations are shown in the bottom left panel, and the fits between the recorded (red) and synthetic (blue) waveforms are shown on the right.

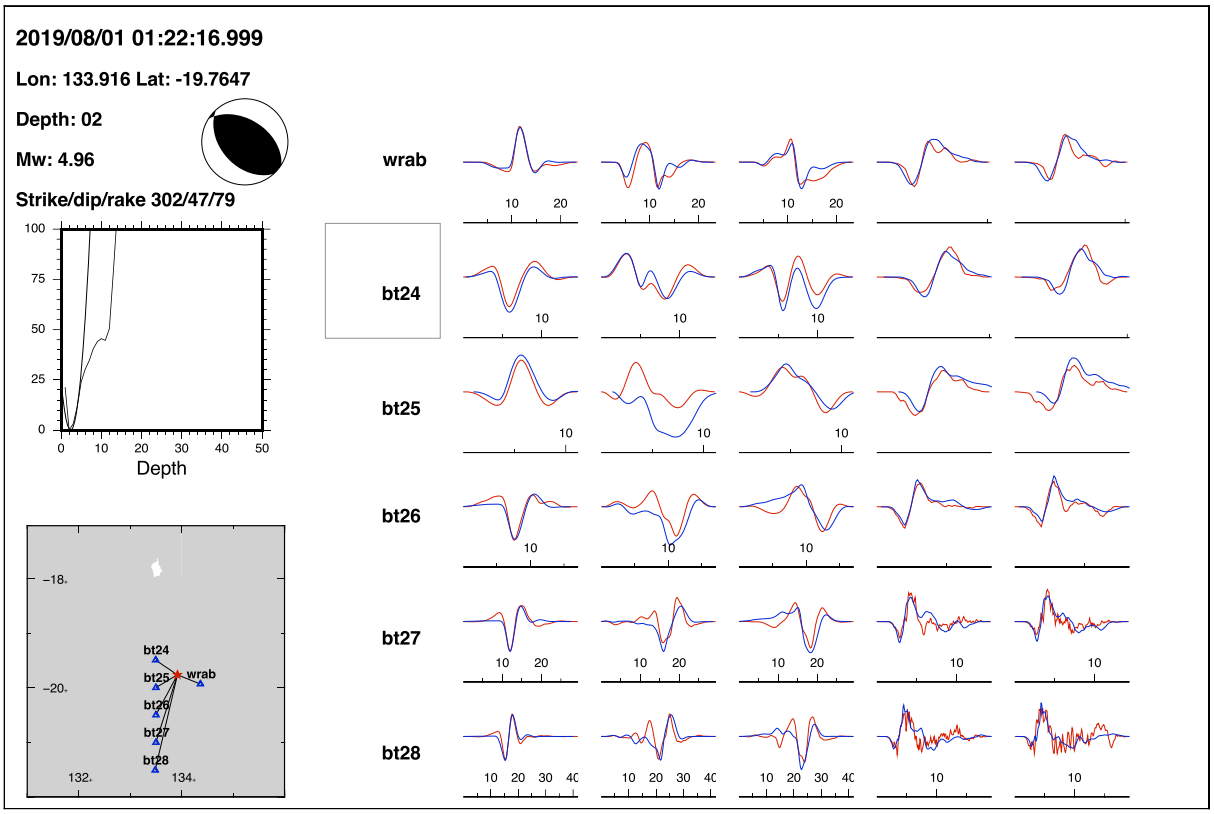

Figure 1. CAP method results for the 2019/08/01 earthquake in the NT.

Table 1. Cratonic region earthquakes used in the GMM development. Metadata for EQIDs 13, 49, and 55 (bold) are from Ghasemi and Allen (2021).

EQID	**M**	Date	Epicenter Longitude (deg)	Epicenter Latitude (deg)	Hypocenter Depth (km)	Strike, Rake, Dip (deg)	Region	No. of Usable 2-component Recordings
61	4.96	2019-08-01	133.916	-19.7647	2	302, 47, 79	Northern Aus Craton	98
59	4.71	2019-05-30	131.85876	-21.28147	5	103, 59, 14	Northern Aus Craton	83
60	3.91	2019-05-30	131.92337	-21.32752	4	101, 64, 3	Northern Aus Craton	85
58	5.34	2018-11-08	116.78733	-34.42316	9	151, 90, 52	Yilgarn Craton	13
53	4.90*	2018-09-16	116.78	-34.43	7	347, 53, 44	Yilgarn Craton	6
44	4.91	2016-07-08	122.511	-32.458	5	331, 37, 59	Yilgarn Craton	6
13	**4.6**	**2020-03-30**	**117.049**	**-30.519**	**0.8**	**-,-,-**	**Yilgarn Craton**	*8*
55	**4.54**	**2018-10-12**	**116.79882**	**-34.39522**	**5.8**	**-,-,-**	**Yilgarn Craton**	*8*
49	**4.13**	**2017-01-03**	**118.455**	**-30.609**	**10**	**-,-,-**	**Yilgarn Craton**	*9*
72	4.39	2010-06-05	136.796	-33.5949	23	0, 62, 51	Gawler Craton	5
82	3.53	2018-07-01	136.7729	-33.618	23	209, 38, 51	Gawler Craton	5
83	4.41	2018-11-21	136.923	-33.2585	33	319, 32, -83	Gawler Craton	5

*The global CMT **M** and depth are 5.3 and 12 km

3 Empirical Calibration

The need to adjust Sea09 is based on evaluations of the performance of the model compared with the earthquake ground motion data. Figure 2a shows an example of this observation for the **M**4.71 earthquake on May 30, 2019. In the top panel, the peak ground acceleration (PGA) versus distance predicted by the Sea09 Cratonic earthquake model is compared with the recordings, where the data are adjusted to the time-averaged shear-wave velocity (V_{s30}) condition of 865 m/s for consistency with Sea09 using the Stewart et al. (2020) site amplification model for stable continental regions. Estimated values of V_{s30} for sites used in this study were compiled by Ghasemi and Allen (2021) and are from three independent sources, in order of preference: Kayen et al. (2015), McPherson (2017); Wald and Allen (2007).

Figure 2a shows that the Sea09 model overpredicts at close distances and underpredicts at large distances. The bottom panel of Figure 2a shows ground motion residuals calculated from the Sea09 model, and the linear trend in these residuals also illustrates the difference in PGA attenuation for this event with that assumed in Sea09. Figure 2b shows a map of the earthquake location and recording sites, along with the boundary between the Northern Australian Craton to the north, and the reactivated Proterozoic crust to the south. Sites within the Cratonic region boundary are filled circles in Figure 2a, and sites outside the boundary are white squares. Similar behaviour is observed for the other Cratonic region events for which we have recorded data. Additionally, the fact that the Sea09 Cratonic ground motion model has a more rapid decay with distance than the non-Cratonic model (not shown), which is the opposite of what we would expect, is an indication that the Cratonic model needs adjustment. Stable continental regions are described by relatively lower effective anelastic attenuation (higher frequency-dependent quality factor) and so high-frequency ground motions have weaker decay with distance at regional distances than active regions (e.g. Baqer and Mitchell, 1998; Bayless, 2021).

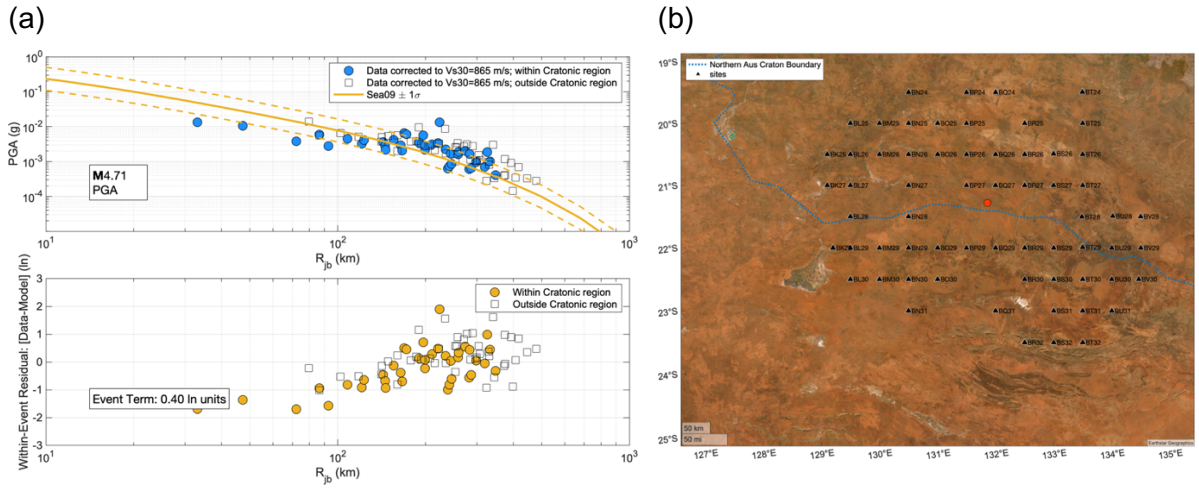

*Figure 2. (a) Evaluation of the Sea09 Cratonic model with ground motion recordings of the May 30, 2019 M4.71 earthquake. Top: PGA versus distance. Bottom: Within-event residuals versus distance. (b) A satellite image map of the May 30, 2019 **M**4.71 earthquake epicentre (red circle) and recording stations (triangles). The blue dashed line represents the boundary between the Northern Australian Craton to the north, and the reactivated Proterozoic crust to the south.*

The basic form of the Sea09 median follows Eq. 1:

$$\ln Sa = c_1 + c_2(\mathbf{M} - m_1) + c_3 \ln R + c_4(\mathbf{M} - m_1)\ln R + c_5 R_{jb} + c_8(8.5 - \mathbf{M})^2 \quad (1)$$

Where $c_3 \ln R$ and $c_4(\mathbf{M} - m_1)\ln R$ represent the magnitude-independent and magnitude-dependent geometric spreading terms, respectively, and $c_5 r$ represents the anelastic

attenuation (Q) term. In the terms that use the logarithm of distance (lnR), Sea09 uses R = $\sqrt{(R_{jb}^2+h^2)}$ where R_{jb} is the Joyner-Boore distance in km and the constant h can be interpreted as a fictitious distance, which causes a flattening of the attenuation curve at very short distances due to the finite rupture dimensions. Sea09 found that a value of 6 km for h provided the best fit both for the Cratonic and Non-Cratonic models.

We update the Sea09 Cratonic model coefficients which control the decay with distance; the geometric spreading and anelastic attenuation model terms. The coefficient c_5 is revised by adding a period-dependent constant δc_5. The value of δc_5 ranges from $\delta c_5 = 0.0015$ at zero period (PGA) to $\delta c_5 = 0.0$ at 10 sec. Increasing c_5 results in more gradual attenuation of the ground motions at distances greater than approximately 80 km (reduced anelastic attenuation). The magnitude-independent geometric spreading coefficient, c_3, is adjusted by adding a period-dependent constant δc_3. The value of δc_3 ranges from $\delta c_3 = 0.2$ at zero seconds period (PGA) and reduces to $\delta c_3 = 0.0$ at ten seconds period, with linear slope in log-period space. Increasing c_3 has the effect of decreasing the attenuation (slope) of the ground motions with distance for distances less than about 80 km. The magnitude-dependent geometric spreading coefficient, c_4, is not modified at this stage because there are not enough large magnitude data to constrain it; the largest Cratonic earthquake with data is about **M**5.2. Finally, the constant c_1 is adjusted by adding $\delta c_1 = -(\delta c_3 + \delta c_5)\ln 100$. The constant adjustment is required because the other two adjustments (δc_3 and δc_5) each increase the predicted ground motion levels for all magnitudes and distances. To balance these, δc_1 hinges the revised model to the Sea09 model values at approximately 100 km distance based on the observation that the model generally does well in this distance range (e.g., Hoult et al., 2021; Bayless et al., 2022). The value of h is unchanged in the adjusted model.

The adjustments described above were set by observation of the attenuation and spectral shapes of the recordings of the earthquakes listed in Table 1. The period-dependence of δc_3 and δc_5 modifies the predicted spectral shape. The change in spectral shape is most pronounced at short distances, where the geometric spreading term dominates the attenuation, and at short periods, where the coefficient modifications are largest. The change in spectral shape is expressed as a reduction of the short period ground motions with minimal change in the long period ground motions.

4 Ground Motions Simulations

Ground motion simulations are used to extrapolate the model to larger earthquake magnitudes that typically control design ground motions but for which no Australian data are available. The earthquake ground motion simulations are validated using the recorded ground motion data. This portion of the Sea09 update is ongoing.

We use the hybrid broadband ground motion simulation methodology of Graves and Pitarka (2015; 2014; 2010; 2004; GP15) as implemented on the Southern California Earthquake Center Broadband Platform, version 19.8 (SCEC BBP; Maechling et al., 2015). The GP15 method combines a deterministic approach at low frequencies (f<1 Hz) with a semistochastic approach at high frequencies (f>1 Hz), where the broadband (0-10 Hz) response is obtained by summing the separate responses in the time domain using matched filters centred at 1 Hz. In GP15 the fault rupture is represented kinematically and incorporates spatial heterogeneity in slip, rupture speed, and rise time by discretising an extended finite-fault into a number of smaller subfaults. The GP15 prescribed slip distribution is constrained to follow an inverse wavenumber-squared fall-off and the average rupture speed is set at a fraction of the local shear-wave velocity, which is then adjusted such that the rupture propagates faster in regions of high slip and slower in regions of low slip. At low frequencies (f<1 Hz), the GP15 methodology contains a theoretically rigorous representation of fault rupture and wave propagation effects and attempts to reproduce recorded ground motion waveforms and amplitudes by summing the response for many point sources distributed across each subfault. At high frequencies (f>1 Hz), GP15 uses a stochastic representation of source radiation, which

is combined with a simplified theoretical representation of wave propagation and scattering effects for each subfault.

Graves and Pitarka (2015) extended their broadband simulation method from active region crustal earthquakes to earthquakes in stable continental regions based on findings from Somerville et al. (2009), Leonard (2010), Beresnev and Atkinson (2002), and with calibration using three eastern North America earthquakes. The modifications included: increasing the average rise time, reducing the average corner frequency, increasing the high frequency stress parameter, using the Leonard (2010) magnitude-area scaling relations, changing the high frequency attenuation (through kappa and Q models), changing the background rupture speed, and removing the shallow and deep weak zones from the rupture characterisation (Graves and Pitarka, 2015). We use these parameter recommendations from Graves and Pitarka (2015) as a starting point and take a trial-and-error approach to refine the parameters based on the simulation and validation of earthquakes in Table 1. A summary of the final parameters and values required by the BBP v19.8 implementation of GP15 will be provided upon completion of the Sea09 update.

The simulations are performed for the events and recording stations listed in Table 1, using the GP method and with the Green's functions described in Bayless et al. (2022). The simulation results for the first event in Table 1 (EQID 61) are presented in this paper. The AusARRAY sites which recorded the EQID 61 earthquake, shown in Figure 3a, are located near or within the Northern Australian Craton region defined in NSHA18, and their site conditions are poorly known. The uncertainties in V_{s30} values and in the site response adjustments are significant and could be reduced in the future with additional data collection or improved models; these sources of uncertainty were similarly identified and accepted in NGA-East (Goulet et al., 2021).

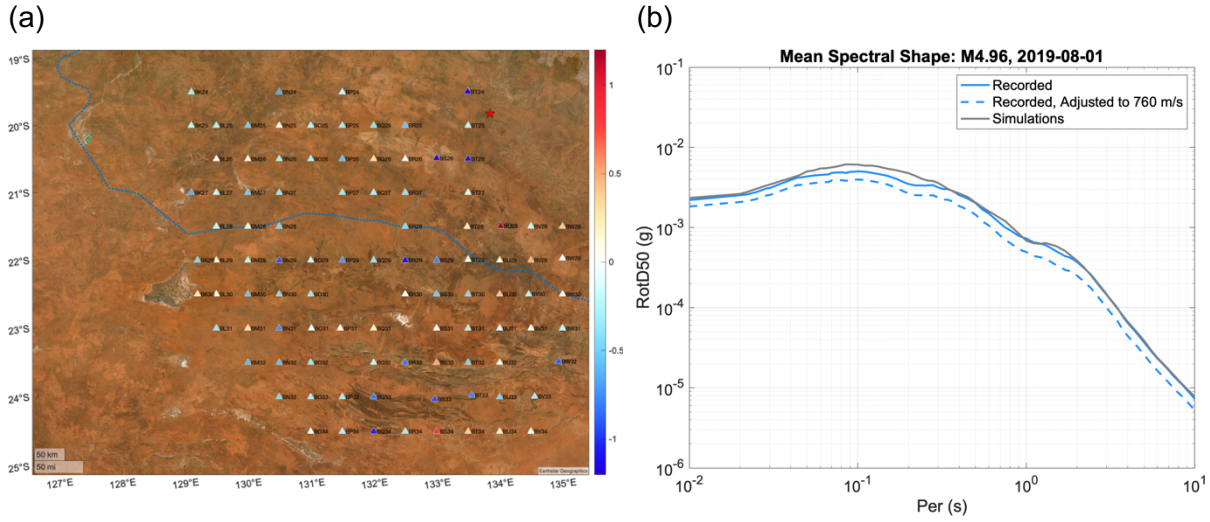

*Figure 3. (a) A satellite image map showing color-coded within-event residuals (EQID 61, **M** 4.96) at the recording sites with less than 600 km hypocentral distance. (b) Mean spectral shapes of all sites within 300 km, showing simulated, recorded, and recorded with adjustment to the V_{s30}=760 m/s site condition.*

For a given spectral period and recording station, the residual is defined as the difference between the natural logarithm of the recorded spectral acceleration (data) and the simulated spectral acceleration, after correcting for site conditions. Figure 3a shows a map of the within-event PGA residuals for this simulation, where negative residuals (cool colours) correspond to simulation over-prediction. Figure 3b shows the mean of spectral acceleration over all sites at each period; this compares the mean spectral shape of the simulations with the data. The dashed blue line in Figure 3b is the mean spectral shape after adjusting each site's recorded response spectrum to the V_{s30}=760 m/s condition using the Stewart et al. (2020) site amplification model for stable continental regions (recommended model with weights for large

impedance contrast and gradual velocity gradient models determined as a function of V_{s30}). The small bump at about 1.5-2 seconds in the response spectra of both the simulations and the recordings is due to the R_g wave, which is caused by a shallow low velocity layer in the crust, and which produces large peak ground velocities. Sea09 observed and modelled this ground motion feature.

Figure 4 shows the distance attenuation of RotD50 spectral acceleration at all sites with less than 300 km rupture distance, for four periods: 0.01 sec (PGA), 0.2 sec, 1 sec, and 4 sec. The Sea09 Cratonic (unmodified model) median plus and minus one standard deviation model predictions are shown, and the circles represent stations inside the Cratonic region boundary, while squares represent stations outside of this boundary. Figure 4 illustrates good agreement in the distance scaling of the simulations with the data from this event.

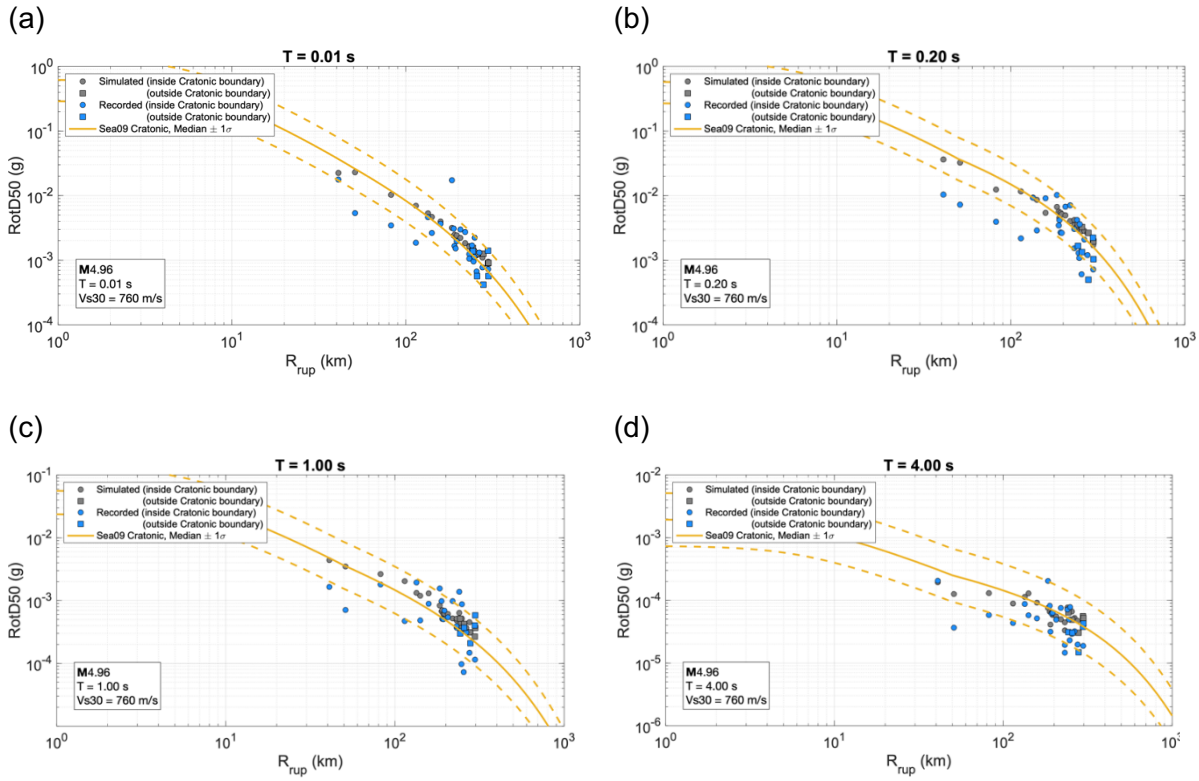

Figure 4. For EQID 61, distance attenuation of recorded (blue) and simulated (grey) RotD50 spectral acceleration at all sites with less than 300 km rupture distance, for four periods: (a) 0.01 sec (PGA), (b) 0.2 sec, (c) 1 sec, and (d) 4 sec.

Figure 5a shows the goodness-of-fit (GOF) summary for this earthquake simulation. The GOF is computed for each spectral period. The mean bias (black line) is the mean residual calculated from all recording stations, using the same definition of residual as defined previously. The red shaded area represents the 90% confidence interval in the mean bias and the green shaded area represents +/- 1 standard deviation among the residuals. The simulation of this event over-predicts the data slightly across all periods without strong period dependence in the mean GOF; the lack of period dependence is encouraging, and a mean bias is generally acceptable if some other events are systematically low, because each event is expected to have an event term. In the final stages of the simulations, the GOF of each event in Table 1 will be compared to determine if the simulations are acceptably calibrated to the recorded data.

Figure 5b shows displacement time series with rupture distance (vertical axis) for the simulations (left) and recordings (right) with less than 300 km rupture distance. Overall, there are strong similarities in the amplitudes, phasing, and durations of the waveforms between the

simulations and the recordings. Postcritical reflections from the lower crust generate the second arrival seen in the simulations at distances of 50 km and less.

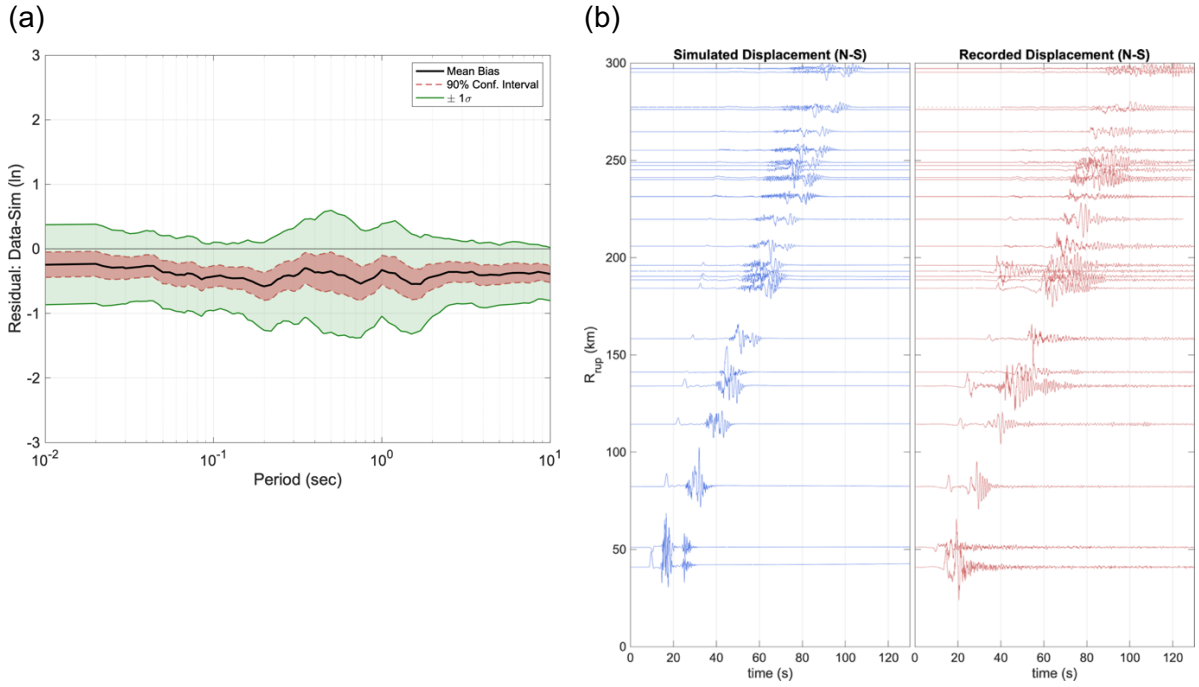

Figure 5. (a) The response spectral goodness-of-fit (GOF) summary for the EQID 61 earthquake simulation. (b) simulated and recorded displacement time series as a function of rupture distance; the vertical scale for displacement amplitudes is the same between both panels of (b).

5 Vertical to Horizontal Spectral Ratio Model

There are no existing V/H spectral ratio models for Cratonic Australia. Using the database of over 30 events compiled in this update, a model for the V/H median and standard deviation is derived using a mixed effects regression (The Math Works, 2022). The model is dependent on **M**, rupture distance (R_{rup}) and the site parameter V_{s30} (Eq. 2). The model is period dependent and applicable to Cratonic Australian earthquakes with **M** from 4 to 8 and for rupture distances from 0 to 500 km. The model adopts the Gülerce and Abrahamson (2011; GA11) magnitude scaling because the limited range of magnitudes in our database did not allow for this component to be determined empirically. The remaining model components are determined empirically. The median model functional form is:

$$\ln(V/H) = a_1 + a_2(\mathbf{M}\text{-}6.75) + [a_3(\mathbf{M}\text{-}6.75)+a_4] \ln R + a_5 \ln(V_1/760) + a_6(8.5\text{-}\mathbf{M})^2 \qquad (2)$$

where ln(V/H) is the natural logarithm of the ratio between the vertical and RotD50 components of spectral acceleration, V_1 is the minimum between V_{s30} and 1100 m/s, and a_1 through a_6 are model coefficients.

In Figure 6, the median V/H ratio from this model is compared with others for a **M**5 scenario at 30 and 200 km distance (left and right columns) and for Vs30 = 270 and 760 m/s (top and bottom rows). The other models in this comparison are Pezeshk et al. (2022; Pea22) for central and eastern North America, GA11 and Bozorgnia and Campbell (2016; BC16) for shallow crustal earthquakes in active tectonic regions, and Ramadan et al. (2021; Rea21) for shallow crustal earthquakes in Italy. As expected, our model is most similar to Pea22, which is for a stable continental region, as compared to the other three models developed for shallow crustal earthquakes in active regions.

Figure 6 shows that, with few exceptions, we observe (and model) larger V/H ratios than the other models. Large vertical component ground motions in Cratonic Australia can be explained by larger angles of incidence in the upper 4 km relative to non-Cratonic regions.

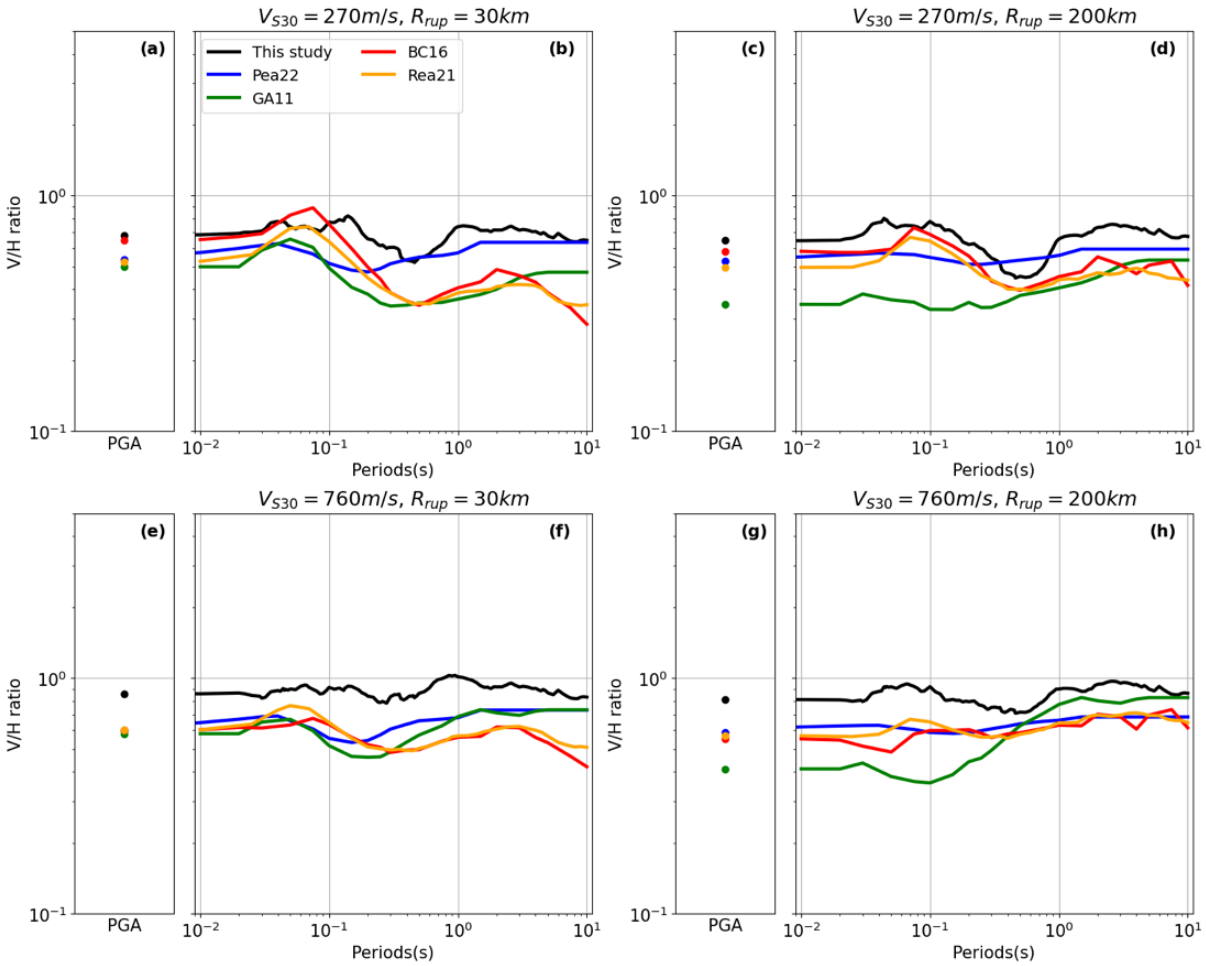

*Figure 6. V/H ratios from this study (black lines) compared with others (coloured lines) at stiff-soil (V_{S30} = 270 m/s, top row) and soft-rock sites (V_{S30} = 760 m/s, bottom row) for **M**5. The left column is for R_{rup} = 30km and right column is for R_{rup} = 200km.*

6 Summary and Future Steps

This paper describes how the Sea09 ground motion model has changed, and as a result how SHA results for engineering projects may be impacted. Comparisons with recently recorded ground motions in Australia have revealed that refinements to the distance and depth scaling components of the model provide a better fit to those data. The Sea09 models are distinct for Cratonic and non-Cratonic region earthquakes. Based on our ongoing evaluations of the newly acquired data, the path and site scaling components of the ground motions from both regions are similar, and most differences are related to source effects. As a result, we propose to update Sea09 with one model which incorporates the earthquake depth; accounting for the effects of R_g waves (from shallow events, impacting longer periods) and for energetic buried ruptures (impacting short periods). This model will be for the median and standard deviation of horizontal component response spectra and V/H ratios.

This update involves broadband strong motion simulations to account for the effects of earthquake source and crustal structure properties of Australia; these are validated using the recorded ground motion data and are used to extrapolate the model to larger earthquake

magnitudes that typically control design ground motions but for which no Australian data are available. These ongoing simulation validations use new data recorded in Cratonic Australia (Ghasemi and Allen, 2021).

The remaining Sea09 updates will be finalized once the validation phase is complete. We will run simulations for suites of scenario events with a range of source depths and kinematic source realizations to develop a simulated ground motion database. Finally, the regression for ground motion model coefficients will be based on the combination of the scenario simulations and the recorded data. At this stage we will also evaluate and potentially adopt models for hanging wall effects and V_{s30} scaling from others (e.g., Abrahamson et al., 2014; Stewart et al., 2020). Finally, we will update the Sea09 model for the aleatory variability based on the available data and on a review of global models (e.g., Al Atik, 2015).

7 Acknowledgements

The authors acknowledge the Center for Advanced Research Computing (CARC) at the University of Southern California for providing computing resources that have contributed to the research results reported within this publication. URL: https://carc.usc.edu. Thanks to Geoscience Australia (in particular, Trevor Allen and Hadi Ghasemi) for making the Cratonic region ground motion and source data publicly available, to David Love for sharing waveform data, first motion data, and magnitudes, focal depths and focal mechanisms of Cleve earthquakes, and to Rob Graves and Arben Pitarka for providing input on the simulations. Hadi Ghasemi and Trevor Allen are thanked for their thoughtful reviews that helped to improve this manuscript.

8 References

Abrahamson, N., W. Silva and R. Kamai (2014). Update of the AS08 Ground-Motion Prediction Equations Based on the NGA-West2 Data Set. Earthquake Spectra: August 2014, Vol. 30, No. 3, pp. 1025-1055.

Al Atik, L. (2015). NGA-East: Ground-Motion Standard Deviation Models for Central and Eastern North America. PEER Report 2015/07. Pacific Earthquake Engineering Center, University of California, Berkeley.

Allen, T.I. (2018). The 2018 National Seismic Hazard Assessment for Australia: Data package: Maps and grid values. Geoscience Australia record 2018/33. Canberra, ACT, Australia

Allen, T., J. Griffin, M. Leonard, D. Clark and H. Ghasemi (2018). The 2018 National Seismic Hazard Assessment: Model overview. Record 2018/27. Geoscience Australia, Canberra. http://dx.doi.org/10.11636/Record.2018.027

ANCOLD (2019). Guidelines for Design of Dams and Appurtenant Structures for Earthquake.

Baqer S, Mitchell BJ (1998) Regional variation of Lg Coda Q in the continental United States and its relation to crustal structure and evolution. Pure and Applied Geophysics 153: 613–638.

Bayless J. (2021). Regional attenuation models in Central and Eastern North America using the NGA-East database. *Earthquake Spectra*. 2021;37: 1460-1486.

Bayless J., P. Somerville, S. Condon, H.K. Thio, H. Ghasemi, T. Allen (2022). Updating the Somerville et al. (2009) Ground Motion Model for Cratonic Australia Using Broadband Ground Motion Simulations of Recently Recorded Cratonic Region Earthquakes. *Proc. of the 2022 Australian Earthquake Engineering Society National Conference.* 24-25 November 2022, Mount Macedon, Victoria, Australia.

Bayless J., P. Somerville, and H.K. Thio (2023). Ground motion modeling updates applicable to seismic hazard assessments for dams in Australia. *Proc. of the Australian National Committee on Large Dams Inc*. (ANCOLD) Conference. 25-27 October 2023, Cairns, Australia

Beresnev, I. A., and G. M. Atkinson (2002). Source parameters of earthquakes in eastern and western North America based on finite-fault modeling, Bull. Seis. Soc. Am. 92, 695–710.

Boore, D.M. (2010). Orientation-independent, nongeometric-mean measures of seismic intensity from two horizontal components of motion. Bulletin of the Seismological Society of America, Vol. 100, No. 4, pp. 1830-1835.

Bozorgnia Y, and Campbell K (2016) Ground Motion Model for the Vertical to Horizontal (V/H) Ratios of PGA, PGV, and Response Spectra. Earthquake Spectra, Volume 32, No. 2, pages 951–978

Ghasemi, H., and T. Allen (2021). Engineering ground-motion database for western and central Australia, Australian Earthquake Engineering Society 2021 Virtual Conference.

Ghasemi, H. and Allen, T. (2018). Selection and ranking of ground-motion models for the 2018 National Seismic Hazard Assessment of Australia: summary of ground-motion data, methodology and outcomes. Record 2018/29. Geoscience Australia, Canberra.

Gorbatov, A., K. Czarnota, B. Hejrani, M. Haynes, R. Hassan, A. Medlin, J. Zhao, F. Zhang, M. Salmon, H. Tkalcic, H. Yuan, M. Dentith, N. Rawlinson, A. Reading, B. Kennett, C. Bugden, and M. Costelloe (2020). AusArray: quality passive seismic data to underpin updatable national velocity models of the lithosphere; In, doi: 10.11636/135284.

Goulet, C.A, Bozorgnia, Y., Kuehn, N., Al Atik, L., Youngs, R.R., Graves, R.W. and Atkinson G.M. (2021). NGA-East Ground-Motion Characterization Model Part I: Summary of Products and Model Development. Earthquake Spectra, 37(S1): 1231–1282. https://doi.org/10.1177/87552930211018723

Graves R. W., Pitarka A. (2004). Broadband time history simulation using a hybrid approach, Proc. 13th World Conf. Earthq. Eng., Vancouver, Canada, paper no. 1098

Graves, R. W., Pitarka, A. (2010). Broadband ground-motion simulation using a hybrid approach, Bull. Seismol. Soc. Am. 100, 2095–2123, doi: 10.1785/0120100057.

Graves R. W., Pitarka A (2015). Refinements to the Graves and Pitarka (2010) Broadband Ground-Motion Simulation Method. Seismological Research Letters; 86 (1): 75–80. doi: https://doi.org/10.1785/0220140101

Gülerce Z, and Abrahamson N (2011) Site-Specific Design Spectra for Vertical Ground Motion. *Earthquake Spectra*, Volume 27, No. 4, pages 1023–1047.

Helmberger, D. V., and G. R. Engen (1980). Modeling the long-period body waves from shallow earthquakes at regional ranges, Bull. Seism. Soc. Am. 70, 1699–1714.

Hoult, Ryan & Pascale, Adam & Jones, Abraham & Allen, Trevor. (2021). The MW 5.9 Woods Point Earthquake: A Preliminary Investigation of the Ground Motion Observations.

Kayen, R. E., B. A. Carkin, T. Allen, C. Collins, A. McPherson, and D. Minasian (2015). Shear-wave velocity and site-amplification factors for 50 Australian sites determined by the spectral analysis of surface waves method, U.S. Geological Survey Open-File Report 2014–1264, pp 118, doi: 10.3133/ofr20141264.

Kottke, A. (2018, July 27). arkottke/pyrotd v0.5.4 (Version v0.5.4). Zenodo. http://doi.org/10.5281/zenodo.1322849

Leonard, M. (2010). Earthquake Fault Scaling: Self-Consistent Relating of Rupture Length, Width, Average Displacement, and Moment Release. Bull. Seis. Soc. Am, 100, 1971-88.

Maechling, P. J., F. Silva, S. Callaghan, and T. H. Jordan (2015). SCEC Broadband Platform: System Architecture and Software Implementation, Seismol. Res. Lett., 86, no. 1

McPherson, A. A. (2017). A revised seismic site conditions map for Australia, Geoscience Australia Record 2017/12, Canberra, doi: 10.11636/Record.2017.012.

Miller, M. S., R. Pickle, R. Murdie, H. Yuan, T. I. Allen, K. Gessner, B. L. N. Kennett, and J. Whitney (2023). Southwest Australia Seismic Network (SWAN): recording earthquakes in Australia's most active seismic zone, Seismol. Res. Lett., doi: 10.1785/0220220323.

Pezeshk S, Farhadi A, and Haji-Soltani A (2022) A New Model for Vertical-to-Horizontal Response Spectral Ratios for Central and Eastern North America. Bulletin of the Seismological Society of America 112 (4): 2018–2030

Ramadan F, Smerzini C, Lanzano G, and Pacor F (2021) An empirical model for the vertical-to-horizontal spectral ratios for Italy. Earthquake Engineering Structural Dynamics. 50:4121–4141.

Somerville, P.G., R.W. Graves, N.F. Collins, S.G. Song, S. Ni and P. Cummins (2009). Source and ground motion models of Australian earthquakes. Proceedings of the 2009 Annual Conference of the Australian Earthquake Engineering Society, Newcastle, Dec 11-13.

Somerville, P. and S. Ni (2010). Contrast in Seismic Wave Propagation and Ground Motion Models between Cratonic and Other Regions of Australia. In Proceedings of the Australian Earthquake Engineering Society, 2010 Conference.

Stewart, J. P., G.A. Parker, G.M. Atkinson, D.M. Boore, Y.M.A. Hashash, and W.J. Silva (2020). Ergodic site amplification model for central and eastern North America. Earthquake Spectra 36 (1), 42-68.

Tan, Y., A Song, S Wei, D Helmberger (2010) Surface Wave Path Corrections and Source Inversions in Southern California. Bulletin of the Seismological Society of America; 100 (6): 2891–2904. doi: https://doi.org/10.1785/0120090063

The Math Works, Inc. (2022). MATLAB (Version 2022a)

Wald, D. J., and T. I. Allen (2007). Topographic slope as a proxy for seismic site conditions and amplification, Bull. Seismol. Soc. Am. 97, 1379-1395, doi: 10.1785/0120060267.

Zhao, L. S., and D. V. Helmberger (1994). Source estimation from broadband regional seismograms, Bull. Seismol. Soc. Am., 84, 91–104.